

Supplementary Information

Length-dependent intracellular bundling of single-walled carbon nanotubes influences retention

Sumin Jin,^{‡a} Piyumi Wijesekara,^{‡b} Patrick D. Boyer,^{‡c} Kris Noel Dahl,^{*c} Mohammad F. Islam^{*a}

^aDepartment of Materials Science and Engineering, ^bDepartment of Biomedical Engineering, ^cDepartment of Chemical Engineering, Carnegie Mellon University, 5000 Forbes Avenue, Pittsburgh, Pennsylvania 15213-3815, USA

‡These authors contributed equally

*Corresponding authors: mohammad@cmu.edu, krisdahl@cmu.edu

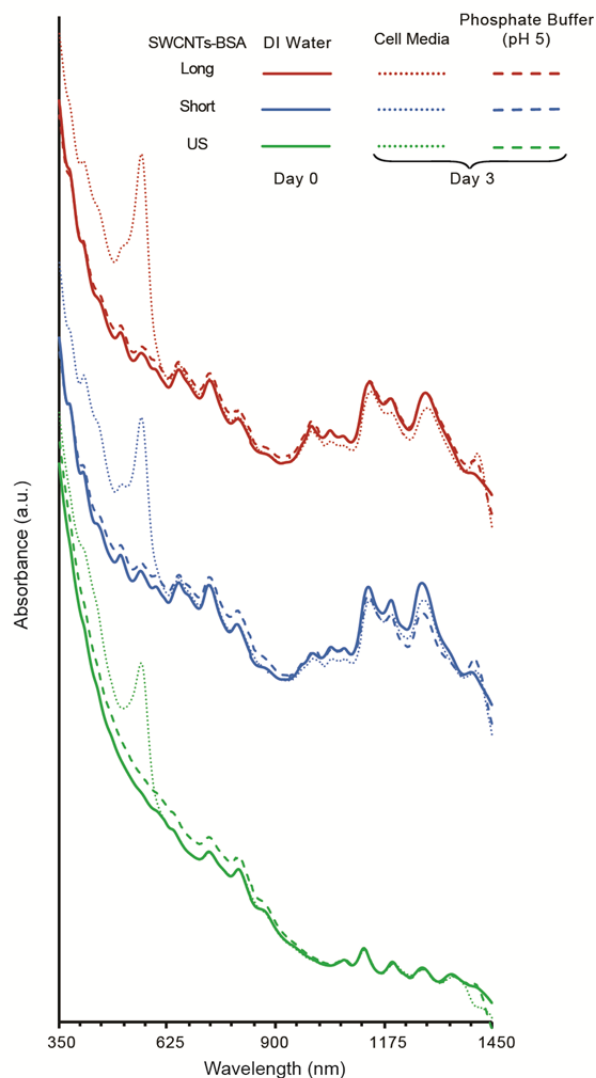


Fig. S1 Comparison of the stability of long-, short-, and US-SWCNTs-BSA in deionized water, cell culture media at 37 °C and phosphate buffer at pH 5 over three days. UV-vis-NIR absorbance spectra from SWCNTs-BSA in cell culture media at 37 °C and in phosphate buffer at pH 5 after day 3 are similar to the same from SWCNTs-BSA in deionized water after day 0. The absorbance spectra from long- and short-SWCNTs-BSA also show sharp van Hove peaks that are indicative of individually dispersed SWCNTs. The peaks in the absorbance spectra from US-SWCNTs-BSA are less pronounced likely due to chemical functionalization of SWCNT surface during acid-based length shortening. The sharp peak at 515 nm in the absorbance spectra of SWCNTs-BSA in cell culture media is from phenol red. All absorbance spectra were normalized to absorbance of each spectrum at 930 nm.

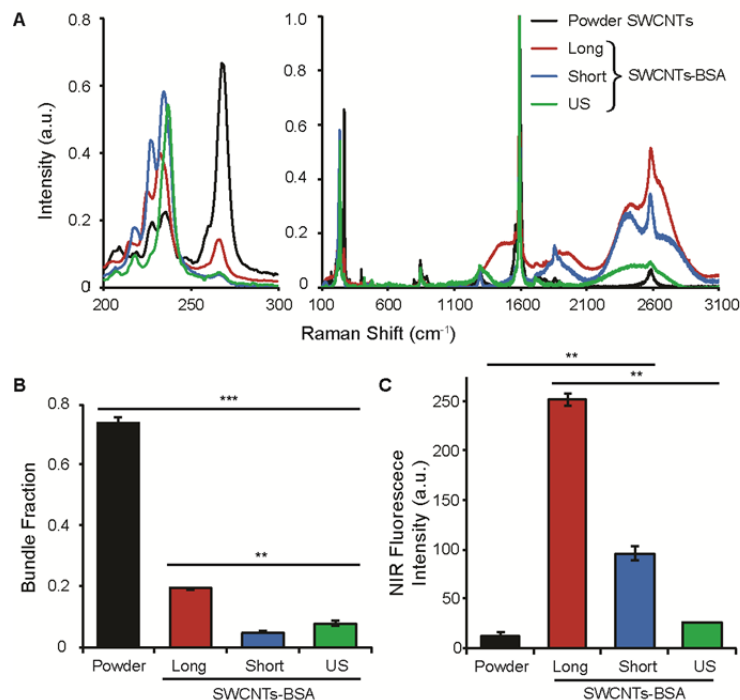


Fig. S2 Optical characterization and quantification of the dispersion state (*i.e.*, individualized *versus* bundled) of long-, short-, and US-SWCNTs-BSA dispersions. (A) The small I_D/I_G (0.03–0.09) of the Raman spectra from SWCNT dispersions confirms that SWCNT structure remains largely intact through the dispersion process. The radial breathing modes (RBMs) over 200–280 cm⁻¹, which are sensitive to the aggregation state of SWCNTs, are magnified in the left panel. RBMs show that US-SWCNTs-BSA do not possess some of the chiralities that are present in long- and short-SWCNTs-BSA, possibly lost during acid-based length shortening. The broad peaks over 1100–3100 cm⁻¹ result from SWCNT fluorescence. (B) The bundle fraction was calculated from maximum RBM intensity > 250 cm⁻¹ normalized to the sum of maximum RBM intensity < 250 cm⁻¹ and > 250 cm⁻¹ for $E_{\text{laser}} = 1.58$ eV (785 nm). All SWCNTs-BSA dispersions have significantly lower bundle fractions than the SWCNT powder. Long-SWCNTs-BSA dispersions contain a significantly higher bundle fraction than short- and US-SWCNTs-BSA, which is likely a result of the gentle dispersion technique utilized to retain longer length SWCNTs. Statistical analysis between indicated samples was performed by unpaired Student's *t*-test; ***p* < 0.01; ****p* < 0.001. (C) The NIR fluorescence intensity was calculated from integrated intensity between 2250–2650 cm⁻¹ normalized to the G-band intensity. Both short- and long-SWCNTs-BSA dispersions provide significantly greater NIR fluorescence than the SWCNT powder and US-SWCNTs-BSA. Statistical analysis between indicated samples was performed by unpaired Student's *t*-test; ***p* < 0.01. Long-SWCNTs-BSA dispersions show greater NIR fluorescence intensity compared to short-SWCNTs-BSA despite possessing greater bundle fraction. US-SWCNTs-BSA dispersions display comparably low NIR fluorescence likely because quantum yield of SWCNTs decreases with length shortening. Data = mean ± SEM from *n* ≥ 2 acquisitions.

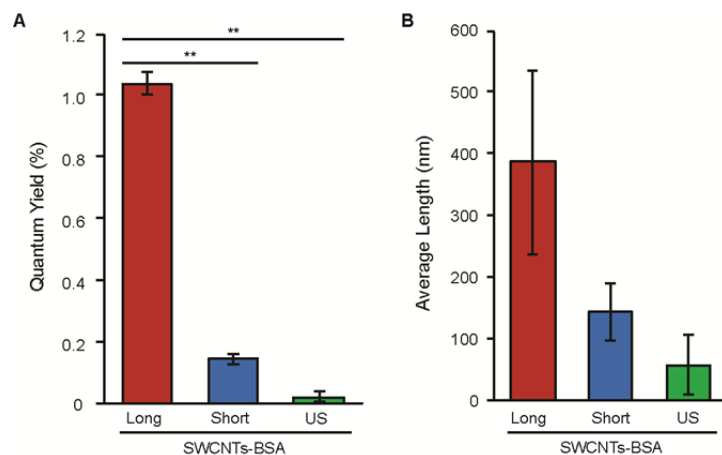


Fig. S3 Average lengths of long-, short-, and US-SWCNTs based on fluorescence quantum yield of their dispersions. Data = mean \pm SEM from $n \geq 3$ acquisitions. (A) Long-SWCNTs-BSA have significantly greater quantum yield than short- and US-SWCNTs-BSA, confirming longer average length. US-SWCNTs-BSA display the lowest quantum yield. Statistical analysis between indicated samples was performed by unpaired Student's *t*-test; $**p < 0.01$. (B) Average SWCNT lengths and length variations calculated using the relationship: quantum yield \propto (SWCNT length)², with quantum yield from length-fractionated short-SWCNTs-BSA (average length 145 ± 17 nm) sample as a reference.¹⁻³

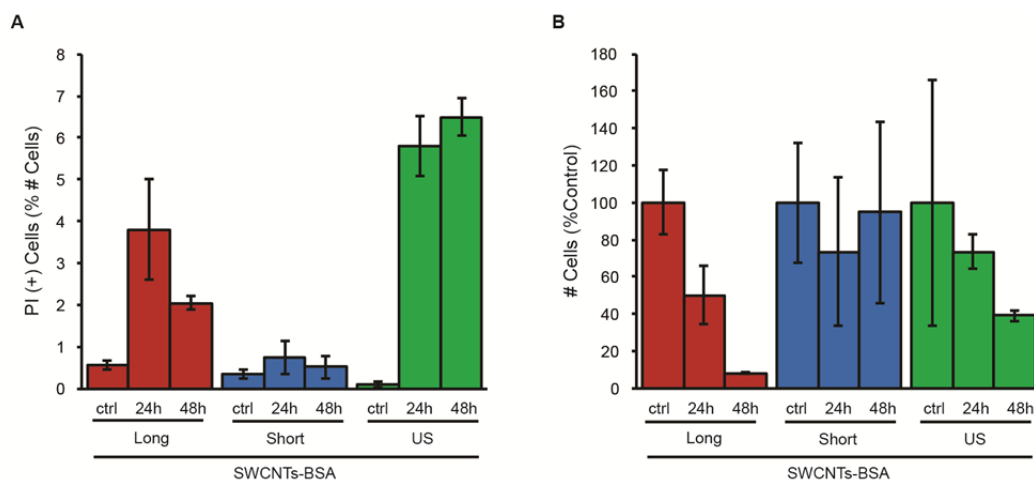


Fig. S4 Dependence of macrophage viability and proliferation on SWCNT lengths. Cells were seeded at 2×10^4 cell cm^{-2} and exposed to long-, short, and US-SWCNTs-BSA for 24 h and 48 h. (A) Viability was measured as a percentage of PI (+) cells with respect to the control. Macrophages do not display significant decrease in viability at 24 h or 48 h for all three lengths of SWCNTs-BSA. (B) Proliferation is represented by the number of cells relative to the control. Macrophages exposed to long-SWCNTs-BSA show the lowest proliferation compared to cells exposed to short- or US-SWCNTs-BSA at both 24h and 48h. Data = mean \pm SEM from $n \geq 5$ fields of view, 1 well.

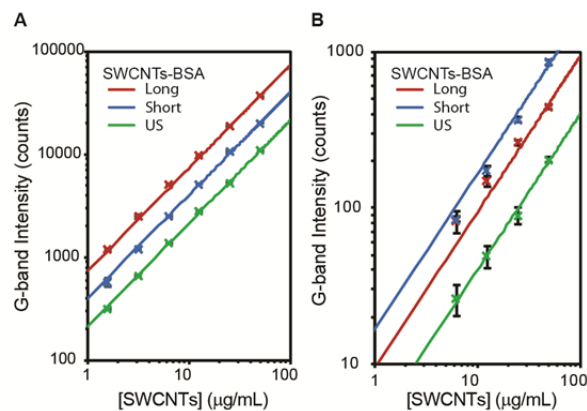


Fig. S5 Standard curves relating SWCNTs-BSA Raman G-band intensity to SWCNT concentration for (A) the 50× (0.75 NA) air immersion objective that was used for cellular uptake, and (B) the 100× (1.4 NA) oil immersion objective that was used for mapping of SWCNT intracellular concentration and distribution experiments. The highest concentration sample was made by diluting SWCNT stock dispersion with known concentration determined using UV-vis-NIR absorbance spectroscopy. The sample was serially diluted and Raman spectra were collected from each diluted sample with an integration time of 60 s for (A) and 2 s for (B). The G-band signal is linear with SWCNT concentration over the indicated concentration ranges. Reproducibility of the measurements of the G-band counts were insured by calibrating to the same silicon standard wafer before each experiment. Data = mean \pm SEM from $n \geq 5$ acquisitions.

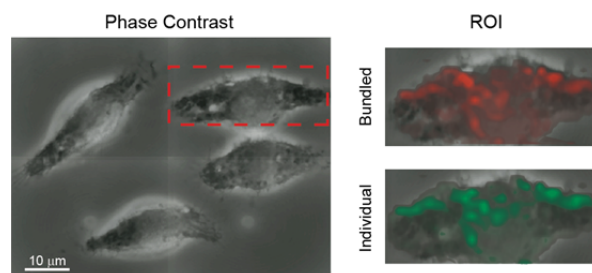


Fig. S6 Intracellular distribution and dispersion state of short-SWCNTs-BSA in macrophages after exposure to comparatively higher concentration of $30 \mu\text{g mL}^{-1}$ (*cf.* Fig. 2). Due to an abundance of phase dense subcellular regions visible in phase contrast images and substantial SWCNT uptake, it is difficult to correlate spatially these regions with Raman spectroscopy mapping results to identify SWCNT dispersion state.

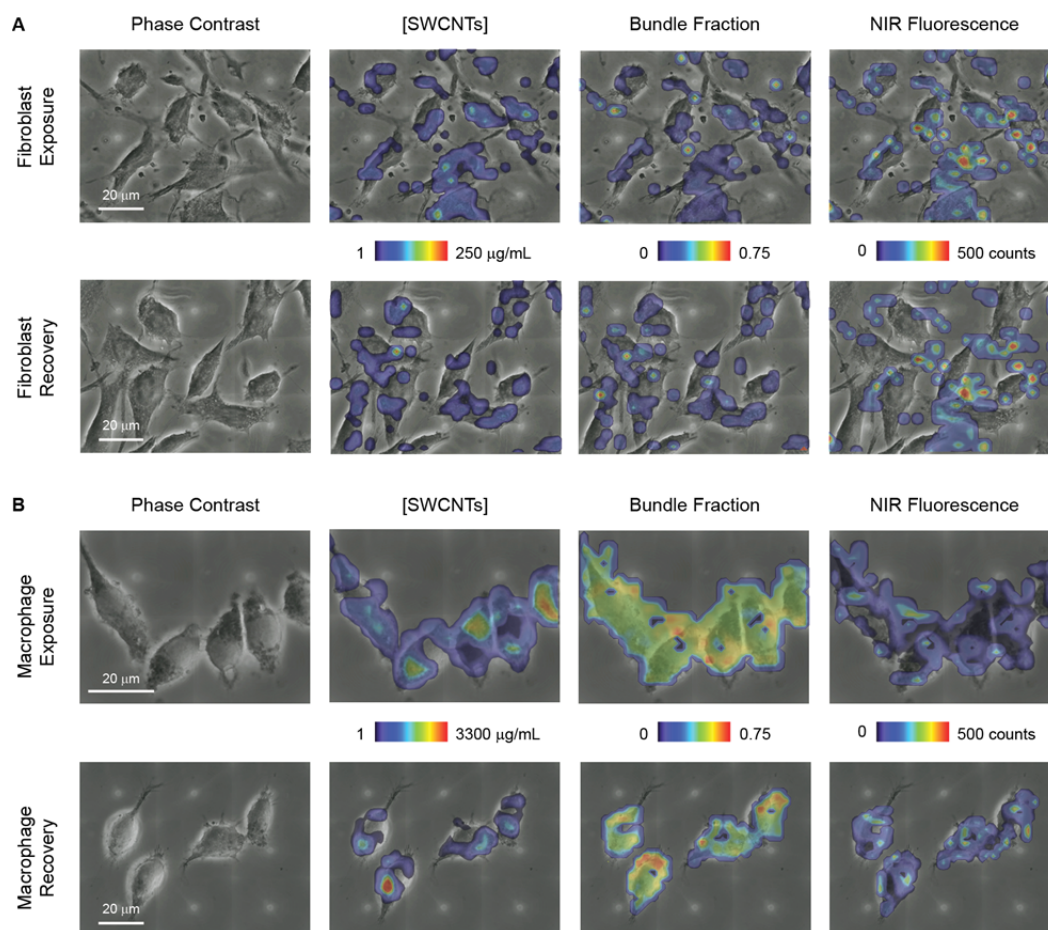


Fig. S7 Subcellular concentration, distribution, and dispersion state of short-SWCNTs-BSA over time in (A) fibroblasts and (B) macrophages. Raman spectroscopy maps of multi-cell fields of view for fibroblasts exposed to $30 \mu\text{g mL}^{-1}$ SWCNTs for 24 h show lower subcellular concentration of SWCNTs with lower bundle fraction and higher NIR fluorescence compared with macrophages. Exposed cells were continued in culture for 24 h without SWCNTs, providing an equal time period for cell recovery. Subcellular SWCNT concentration decreases with reduced bundle fraction but the NIR fluorescence slightly increases in fibroblasts after recovery. On the other hand, the intracellular SWCNT concentration, the bundle fraction, and the NIR fluorescence are nearly unchanged in macrophages after recovery.

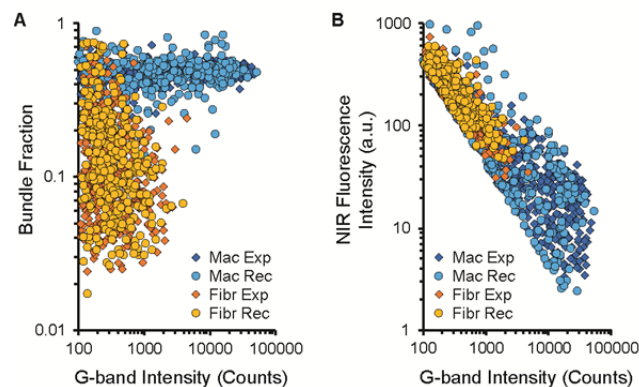


Fig. S8 Comparison of the bundle fraction and the NIR fluorescence intensity for every imaged voxel of short-SWCNTs-BSA in fibroblasts and macrophages that were exposed to $30 \mu\text{g mL}^{-1}$ SWCNTs for 24 h and then recovered for 24 h. (A) For exposure, bundling in macrophages appears to be independent of intracellular SWCNT concentration but show weak linear dependence in fibroblasts. The bundle fractions in both fibroblasts and macrophages show almost no change after recovery. (B) The NIR fluorescence intensity shows intracellular SWCNT concentration dependent linear trend for both fibroblasts and macrophages. For fibroblasts, the fluorescence intensity distribution show slight broadening after recovery. In contrast, intracellular SWCNT concentrations in macrophages do not change appreciably after recovery. $n \geq 630$ (320) and 560 (290) voxels for exposure (recovery) for fibroblasts and macrophages, respectively.

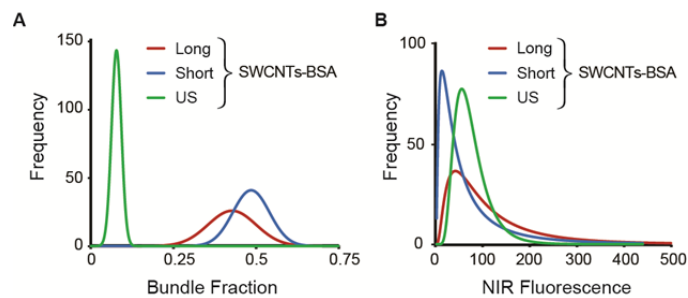


Fig. S9 Distributions of (A) the SWCNT bundle fraction and (B) the G-band normalized integrated SWCNT NIR fluorescence intensity taken across multiple macrophages ($n \geq 2$ fields of view) for SWCNTs-BSA with all three lengths. Short-SWCNTs-BSA in macrophages have higher bundling with lower NIR fluorescence compared with US- and long-SWCNTs-BSA. The lines represent Gaussian and logarithmic fits to the distributions of the bundle fraction and the NIR fluorescence, respectively.

References

- 1 A. Rajan, M. S. Strano, D. A. Heller, T. Hertel and K. Schulten, *Journal of Physical Chemistry B*, 2008, **112**, 6211-6213.
- 2 M. F. Islam, E. Rojas, D. M. Bergey, A. T. Johnson and A. G. Yodh, *Nano Letters*, 2003, **3**, 269-273.
- 3 B. D. Holt, P. A. Short, A. D. Rape, Y.-I. Wang, M. F. Islam and K. N. Dahl, *ACS Nano*, 2010, **4**, 4872-4878.